Journal of Materials Chemistry C

Enhancing thermal stability of n-type conduction in carbon nanotubes via cation replacement mediated by bicyclic guanidinium salts

Journal:	*Journal of Materials Chemistry C*
Manuscript ID	TC-ART-03-2025-001263.R1
Article Type:	Paper
Date Submitted by the Author:	20-May-2025
Complete List of Authors:	Kawasaki, Kaho; Kobe University Nishinaka, Mayuko; Kobe University Koshiba, Yasuko; Kobe University, Chemical Science and Engineering Akiyama, Azumi; Kobe University Wei, Qingshuo; National Institute of Advanced Industrial Science and Technology (AIST), Nanosystem Research Institute (NRI) Funahashi, Masahiro; Kobe University, Department of Chemical Science and Engineering Horike, Shohei; Kobe University, Department of Chemical Science and Engineering

ARTICLE

Enhancing thermal stability of n-type conduction in carbon nanotubes via cation replacement mediated by bicyclic guanidinium salts

Received 00th January 20xx,
Accepted 00th January 20xx

DOI: 10.1039/x0xx00000x

Kaho Kawasaki,[a] Mayuko Nishinaka,[a] Yasuko Koshiba,[a,b] Azumi Akiyama,[a,b] Qingshuo Wei,[c,d] Masahiro Funahashi,[*,a,b] Shohei Horike,[*,a,b,c,e]

The development of thermally stable n-type carbon nanotubes (CNTs) is crucial for their implementation in pn junction devices. In previous work, we introduced an ion replacement technique to stabilize chemically p-doped CNTs, demonstrating the control of hole density and the stabilization of doped states through separate doping and anion replacement processes. This study extends the methodologies to n-type doping by substituting the cation with a specific dopant or stabilizer. The exceptional reduction capability of the cobalt-based complex was evident from the negative Seebeck coefficient, the markedly high electrical conductivity, and the reduction in work function of the doped CNTs. Additionally, the selection of the anion is critical for successful cation replacement, as explored through complex chemistry perspectives. The n-type CNTs, coordinated with bicyclic guanidinium cations, showed improved thermal stability compared to their as-doped counterparts. Lastly, we discuss the thermoelectric properties (with the power factor up to 100 μW m^{-1} K^{-2}) as prospective applications for n-type CNTs in energy harvesting. This foundational work proposes a strategy for engineering n-type CNTs with optimized doping levels and enhanced stability.

Introduction

Traditionally dependent on inorganic materials, the field of electronics has shifted toward exploring organic alternatives that offer robust performance and stability. Carbon nanotubes (CNTs) have garnered significant interest as viable candidates for electronic,[1] optoelectronic,[2] and energy devices,[3] owing to their high carrier mobility,[4] distinct features in the density of states of electron,[5] tunable polarity (p- and n-type),[6] and substantial Seebeck coefficients.[7] Initial investigations in the 1990s into CNT properties were predominantly theoretical,[8–10] constrained by the challenges of acquiring quality CNT samples. However, advancements in synthetic methods for producing high-quality CNTs on a bulk scale,[11–13] along with improved techniques for segregating semiconducting from metallic tubes,[14–16] have catalyzed experimental research since the 2000s. This research has vigorously pursued the exploration of physicochemical properties and device engineering, bringing theoretical concepts to practical realization.

Furthermore, the development of pn junction devices using CNTs critically depends on the selection of the major carrier type and the optimization of its density. The chemical doping of CNTs involves charge-transfer interactions between the CNTs and either oxidants (for p-type) or reductants (for n-type) that possess suitable redox potentials. Naturally occurring CNTs tend to exhibit p-type characteristics due to electron withdrawal by O_2 impurities in air (autoxidation).[17] To date, a variety of dopants have been introduced to modulate the polarity of CNTs. For example, protonic acids,[18,19] halogen gases,[20] superacids,[21] and $AuCl_3$[22] have served as oxidants, while alkali metals,[23] amine and imidazole derivatives,[24,25] superbases,[26,27] and crown ether complexes[28] have functioned as reductants. Techniques such as optical absorption,[29] work-function shifts,[30] and thermoelectric assessments[31] have been utilized to detail the impacts of carrier doping.

However, adjusting the polarity of CNTs through the use of redox-active chemicals does not necessarily yield materials ready for practical device applications. Typically, the doped states of CNTs are vulnerable to environmental factors such as air, humidity, and heat. Thermal stability is particularly critical, as many devices experience significant heating during operation due to currents in transistors,[32] light exposure in photodetectors,[33] and prolonged thermal exposure in thermoelectric generators. Notably, n-doped CNTs are highly

[a] *Department of Chemical Science and Engineering, Graduate School of Engineering, Kobe University, 1-1 Rokkodai-cho, Kobe 657-8501, Japan*
[b] *Research Center for Membrane and Film Technology, Kobe University, 1-1 Rokkodai-cho, Kobe 657-8501, Japan*
[c] *Research Institute of Core Technology for Materials Innovation, Department of Materials and Chemistry, National Institute of Advanced Industrial Science and Technology (AIST), 1-1-1 Higashi, Tsukuba, Ibaraki 305-8565, Japan*
[d] *Graduate School of Pure and Applied Science, University of Tsukuba, 1-1-1 Tennodai, Tsukuba, Ibaraki 305-8577, Japan*
[e] *Center for Environmental Management, Kobe University, 1-1 Rokkodai-cho, Kobe, 657-8501, Japan*
*Corresponding author.
Tel: +81-78-803-6150. Email: funahashi.masahiro@phoenix.kobe-u.ac.jp (Masahiro Funahashi).
Tel: +81-78-803-6194. Email: horike@crystal.kobe-u.ac.jp (Shohei Horike).

Supplementary Information available: Chemicals and Materials; NMR data; Thermal stability data; Comparison of thermoelectric power factors. See DOI: 10.1039/x0xx00000x

unstable at elevated temperatures, which often leads to rapid p-type reversion (dedoping).[34] Efficient electron doping and the stabilization of these doped states are crucial for the effective integration of CNTs into functional devices.

Chemically p- or n-doped CNTs acquire positive or negative charges that are electrostatically balanced by the anions or cations (conjugate bases or acids) introduced by the dopants. Therefore, the stability of these complexes is critical to maintaining the doped states of the CNTs. Our previous research demonstrated that doping with bicyclic guanidine superbases and their derivatives produces thermally stable n-type CNTs.[26] The excellent adsorption properties of the cations and radical cations from the base to the negatively charged CNTs, due to their rigid planar molecular structures, contribute to their remarkable stability, as supported by computational studies.[35]

Recent advancements have shown that ion replacement processes offer a viable method for chemically doping π-conjugated molecules and CNTs.[36–40] Moreover, we have recently established that anion replacement effectively induces stable p-type conduction in CNTs, capable of withstanding long-term exposure to air for over a year.[41] Even when p-doped CNTs are inherently unstable, the induced conductive properties can be maintained by substituting the coordinated anions (originally provided by the dopants) with stabilizer anions, as schematically depicted in Fig. 1a. This method facilitates the optimization of doping levels during chemical doping and ensures the stability of the doped states by subsequent anion replacement.

In this study, we extend our methodology to include n-type doping through cation replacement as depicted in Fig. 1b. We utilized bis(pentamethylcyclopentadienyl)cobalt(II) ($CoCp^*_2$; shown in Fig. 2a), known for its very shallow oxidation potentials, to facilitate the injection of high-density electrons into the CNTs. Additionally, we explored salts composed of a protonated 1,5,7-triazabicyclo[4.4.0]dec-5-ene superbase cation ($TBDH^+$) combined with various anions, including chloride (Cl^-), nitrate (NO_3^-), and bis(trifluoromethanesulfonyl)imide ($TFSI^-$), as depicted in Fig. 2b–d—as agents for cation replacement. The effectiveness of this cation replacement strategy was verified by observing the transient changes in the thermoelectric properties of both doped and cation-replaced CNTs during incubation periods. This conceptual approach lays the foundation for developing n-type CNTs with enhanced doping precision and stability.

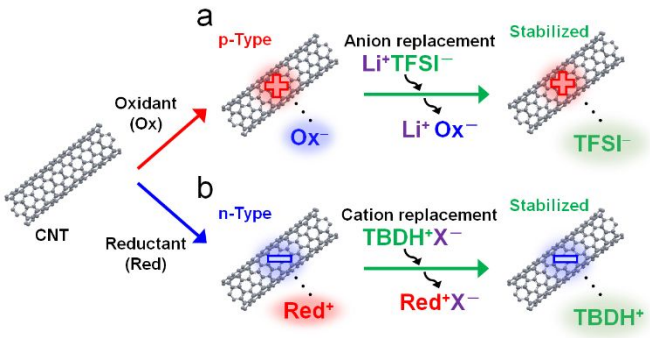

Fig. 1 Schematic diagrams illustrating (a) chemical p-type doping and anion replacement, and (b) chemical n-type doping and cation replacement on CNTs. Li-TFSI was previously identified as an effective stabilizer for p-type CNTs. In this study, we investigate the stabilizing capabilities of TBDH-based salts for n-type CNTs.

Experimental Method

Chemicals and Materials

The chemicals and materials utilized in this study are detailed in Table S1, including their purities and sources.

Synthesis of Electrolytes Containing TBDH cation

The synthesis procedure for each salt followed methods similar to those described in our previous work.[35] TBD was dissolved in deionized water to a concentration of 66.6 mg mL^{-1}. Aqueous solutions of HCl and HNO_3 were added dropwise into the 15 mL of the TBD solution until the pH reached 6–7, indicating neutralization of TBD. The mixtures were then incubated overnight at 100 °C in air to facilitate water evaporation, yielding TBDH-Cl and TBDH-NO_3 as white solids. For the synthesis of TBDH-TFSI, a 15 mL aqueous solution of TBD (66.6 mg mL^{-1}) was neutralized with HNO_3, followed by the addition of equimolar amounts of Li-TFSI. The solution was stirred overnight at 100 °C in air, during which it separated into an upper aqueous phase containing $LiNO_3$ and a lower oil phase containing TBDH-TFSI. The oil phase was isolated, washed three times with deionized water, and dried at 100 °C in air overnight to eliminate any remaining water.

Film Formation

Self-standing CNT films, approximately 16 mm in diameter and 30 µm thick, were fabricated by vacuum filtration of an aqueous CNT dispersion, as per the protocols outlined in our previous publications .[26,41]

Doping and Cation Replacement

After purging acetonitrile with N_2 gas at 45 °C for 60 min,

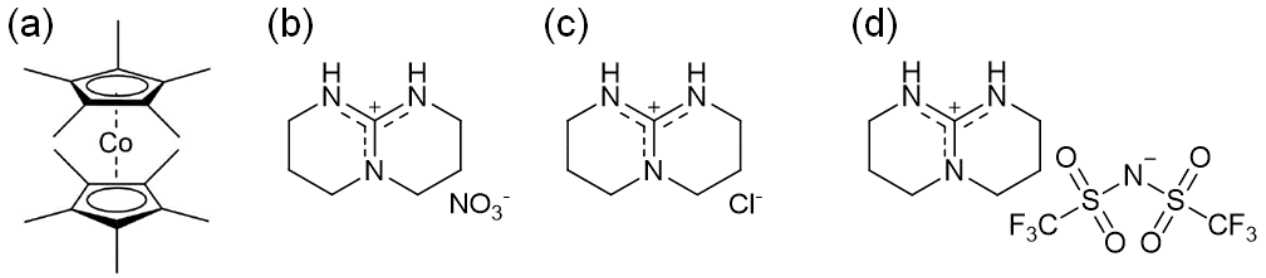

Fig. 2 Chemical structures of (a) $CoCp^*_2$, (b) TBDH-Cl, (c) TBDH-NO_3, and (d) TBDH-TFSI.

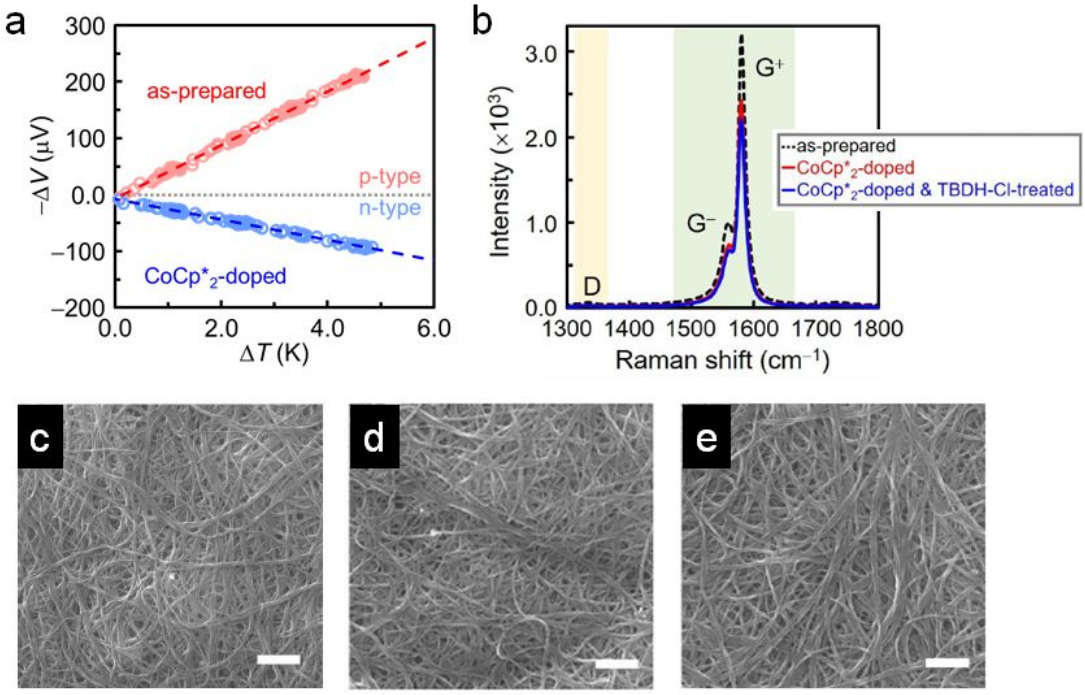

Fig. 3 (a) Output voltage ($-\Delta V$) as a function of temperature difference (ΔT) for as-prepared and $CoCp^*_2$-doped CNT films, where the slope indicates the Seebeck coefficient. (b) Raman spectra of as-prepared, $CoCp^*_2$-doped, and $CoCp^*_2$-doped followed by TBDH-Cl treatment of CNT films. SEM images of (c) as-prepared, (d) $CoCp^*_2$-doped, and (e) $CoCp^*_2$-doped followed by TBDH-Cl treatment of CNT films. Scale bars represent 1 μm.

$CoCp^*_2$ was dissolved in the acetonitrile at a concentration of 2.5 mM. The self-standing CNT films were then immersed in a 20 mL solution of $CoCp^*_2$ in acetonitrile at 40 °C for 30 min, followed by drying at 60 °C for 10 min. Doped CNT films were subsequently immersed in 3 mL acetonitrile solutions of TBDH-Cl, TBDH-NO_3, or TBDH-TFSI (0.1 M) at room temperature for 5 min, and then dried at 60 °C for 10 min. All processes were conducted in a glove box under a controlled atmosphere with a relative humidity below 15%, maintained by a flow of N_2 gas.

Characterizations

All measurements were conducted at approximately 298 K in air. The methods for assessing the Seebeck coefficient, four-probe electrical conductivity, and surface potential are detailed in our earlier publications.[26,27,35,41] The shift in the work function was derived from changes in the surface potential. For thermal stability assessments, the CNT films were incubated at 100 °C in air using an SU-222 system (ESPEC). Observations via scanning electron microscopy (SEM) and energy-dispersive X-ray spectroscopy (EDS) analyses were performed with a JSM-7100 and JED-2300 (JEOL), respectively. Raman spectra were captured using an NRS-7100 (JASCO). Proton nuclear magnetic resonance (^{1}H NMR) spectra of deuterated chloroform solutions of TBD and TBDH-Cl were obtained with a JNM-ECZS spectrometer (JEOL).

Results and Discussion

Doping Effect of $CoCp^*_2$

For the experimental investigations, round-shaped, self-standing films, approximately 16 mm in diameter and 30 μm thick, were fabricated from single-walled CNTs averaging 1.6 nm in tube diameter and utilized for all characterizations. The Seebeck coefficient and electrical conductivity were measured to identify the predominant carrier types within the CNTs both before and after the doping and cation replacement processes. The polarity of the material, indicated by the sign of the Seebeck coefficient, distinguishes between p- and n-type carriers. Moreover, a complementary relationship is observed between each parameter and the carrier density;[42] typically, an increase in carrier density leads to higher electrical conductivity and a reduction in the absolute value of the Seebeck coefficient, thus facilitating the assessment of changes in carrier density.

The Seebeck coefficient (S) was determined from the output voltage (ΔV) generated under an applied temperature difference (ΔT) as follows:

$$S = -\frac{\Delta V}{\Delta T}. \quad (1)$$

The Seebeck coefficient of the as-prepared film, as calculated from the slope of the $-\Delta V$ versus ΔT plots shown in Fig. 3a, is approximately +45 μV K^{-1}. The positive sign indicates a p-type nature, primarily due to the autoxidation of the CNTs in air.[17] The four-probe electrical conductivity of the same samples was approximately 1690 S cm^{-1}.

For n-type doping, the as-prepared CNT films were immersed in an acetonitrile solution containing $CoCp^*_2$. Post-doping, the slope of the $-\Delta V$ versus ΔT plots shifted to negative,

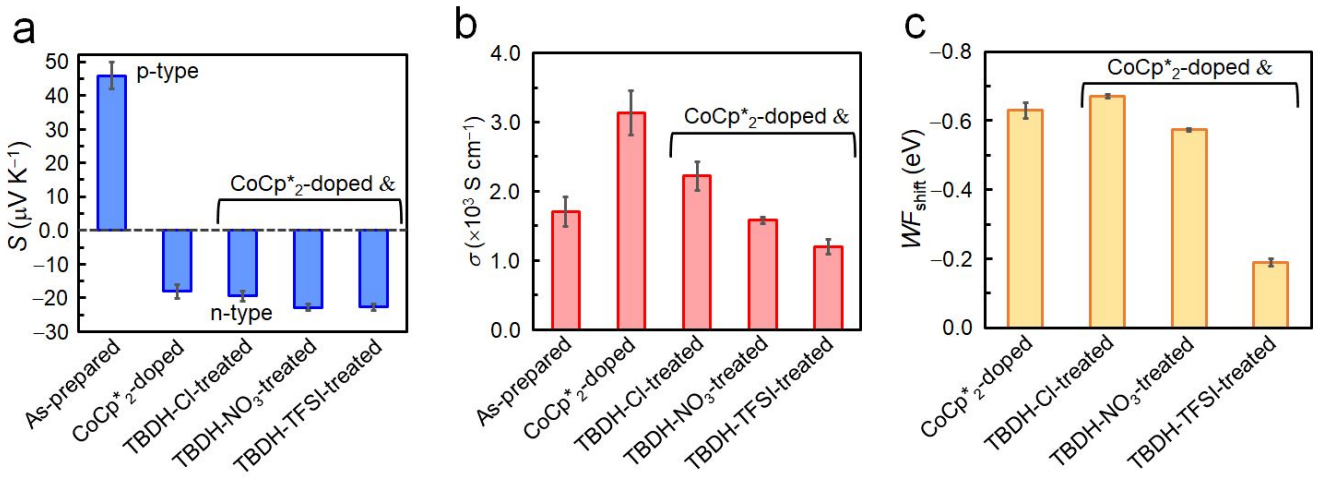

Fig. 4 Variations in (a) Seebeck coefficient (S), (b) electrical conductivity (σ), and (c) work function shift (WF_{shift}) for CoCp*$_2$-doped and TBDH-X ($X^- = Cl^-$, NO_3^- or $TFSI^-$) treated CNT films. Data statistics: $n \geq 3$; error bars represent SDs.

signifying a transition of the major carrier species from holes to electrons. Moreover, the electrical conductivity significantly increased to 3130 S cm^{-1}. This observation, coupled with the decreased absolute value of the Seebeck coefficient, suggests that CoCp*$_2$ introduces electrons into the CNTs at a higher density than the original holes. Notably, the electrical conductivity of the CoCp*$_2$-doped CNTs substantially exceeds that of previously reported n-doped CNTs (for example, 1600 and 1301 S cm^{-1} for TBD- and polyethyleneimine (PEI)-doped CNTs, respectively)[26,43], and even surpasses that of electrochemically doped CNTs achieved by applying a potential of −1.5 V versus Ag/Ag$^+$ in an electrolyte,[35] demonstrating the potent n-doping capability of CoCp*$_2$.

Raman spectra in the G- and D-band regions (Fig. 3b) and SEM images (Fig. 3c,d) indicate that there were no structural deformations in the sp^2 configurations of the CNTs or alterations in the bundle structures, suggesting that the enhanced conductivity is primarily due to an increase in electron density. This conclusion is supported by the G$^+$/D ratio variations listed in Table 1, which confirm minimal covalent modifications to the tubes.

Table 1 G$^+$/D ratios of as-prepared, CoCp*$_2$-doped, and CoCp*$_2$-doped followed by TBDH-Cl treatment of CNT films, extracted from the data shown in Fig. 3b.

Sample	G$^+$/D ratio
As-prepared	42±6.5
CoCp*$_2$-doped	60±4.4
CoCp*$_2$-doped and TBDH-Cl-treated	60±1.6

Data statistics: n = 3. The error indicates the corresponding standard deviation (SDs).

The oxidation potential of CoCp*$_2$ is −1.54 V versus the normal hydrogen electrode (NHE),[44] which corresponds to approximately −2.9 eV versus the vacuum level. This relatively shallow oxidation potential facilitates high-density electron injections into the CNTs via a Co^{2+} to Co^{3+} valence change. For comparison, the redox potential of a well-known reducing agent for organic semiconductors, bis(cyclopentadienyl)cobalt(II) ($CoCp_2$), is −0.93 V versus NHE.[44] CoCp*$_2$ with its methyl-groups-functionalized Cp moieties, exhibits significantly greater reducing capabilities than $CoCp_2$ due to the inductive effect.[45] This potent doping capacity is further demonstrated by the reduction of the work function in the CNTs to −620 meV post-doping, representing a more substantial negative shift compared to the change observed in electrochemically doped CNTs (less than −200 meV) achieved by applying a potential of −1.5 V versus Ag/Ag$^+$ in an electrolyte (approximately −3.7 eV versus the vacuum level).[35]

Cation Replacement and Thermal Stability

In this study, we synthesized TBDH-X (X = Cl^-, NO_3^-, and $TFSI^-$) as cation replacement reagents, as depicted in Fig. 2b–d. Fig. S1 in the Electronic Supplementary Information (ESI†) presents the ^{1}H NMR spectra. To explore the impact of cation replacement, the CoCp*$_2$-doped CNT films were treated with acetonitrile solutions of TBDH-Cl, TBDH-NO_3, and TBDH-TFSI. Post-treatment, the Raman spectra (Fig. 3b), G$^+$/D ratio (Table 1), and the bundle structures as observed by SEM (Fig. 3e) revealed no significant alterations when compared to the as-prepared and CoCp*$_2$-doped samples.

Fig. 4a depicts the variations in the Seebeck coefficients of the CNT films following different treatments. The negative signs were maintained after treatments with TBDH-based salts, but there was a slight increase in the absolute values, indicative of a dedoping tendency. The use of acetonitrile as the solvent may contribute to this dedoping effect. The changes in electrical conductivity, as displayed in Fig. 4b, clearly support this trend, particularly for the TBDH-TFSI-treated samples. The negative shifts in work function achieved through CoCp*$_2$ doping were diminished following salt treatment, as evidenced in Fig. 4c. This reduction was particularly notable in the TBDH-TFSI-treated

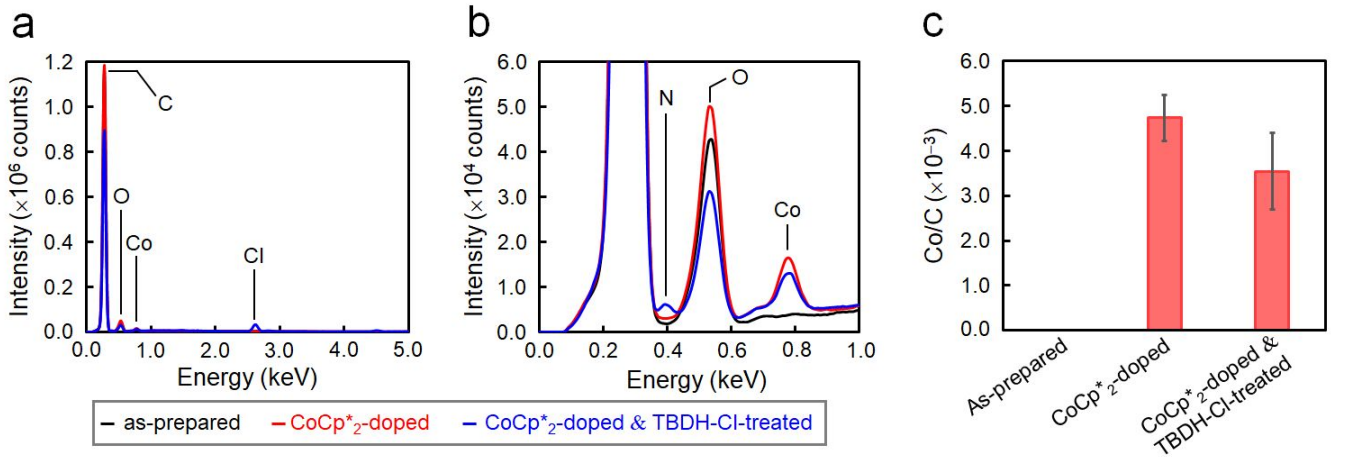

Fig. 5 (a) EDS spectra of as-prepared, CoCp*$_2$-doped, and CoCp*$_2$-doped followed by TBDH-Cl treatment of CNT films. (b) Enlarged view of panel (a). (c) Compositional ratios of cobalt to carbon (Co/C) in as-prepared, CoCp*$_2$-doped, and CoCp*$_2$-doped followed by TBDH-Cl treatment of CNT films, derived from the data in panel (a). Note: N/C ratio could not be quantified due to weak N-related signal intensity. Data statistics: $n = 3$; error bars represent SDs.

samples. Conversely, the TBDH-Cl- and TBDH-NO_3-treated CNT films maintained a negative Seebeck coefficient (approximately −20 μV K^{-1}), relatively high electrical conductivity (1,500–2,200 S cm^{-1}), and a substantial negative shift in work function (approximately −600 meV), suggesting that these salt solutions enhance the stabilization of the n-doped CNTs through effective cation replacement.

The variability in cation replacement effectiveness can be interpreted through the lens of the hard and soft acids and bases (HSAB) theory.[46] The chemical interactions and cation replacement dynamics can be schematized as follows:

$$\mathrm{CNT} + \mathrm{CoCp^*_2(II)} \rightarrow \mathrm{CNT^-{:}CoCp^*_2(III)}. \quad (2)$$

$$\mathrm{CNT^-{:}CoCp^*_2(III)} + \mathrm{TBDH^+{:}X^-} \rightarrow \mathrm{CNT^-{:}TBDH^+} + \mathrm{CoCp^*_2(III){:}X^-}. \quad (3)$$

In this context, efficient coordination between CoCp*$_2$(III) and anions X$^-$ is crucial for facilitating cation exchange (favoring the rightward reaction in Eq. (3)). Co^{3+} is considered a relatively hard cation according to the HSAB theory[47] and tends to stabilize through coordination with hard species. Therefore, Cl$^-$ and NO_3^- (hard anions) promote the replacement of CoCp*$_2$ with TBDH$^+$ effectively, whereas TFSI$^-$ (a relatively soft anion) does not readily engage in coordination with CoCp*$_2$(III).

Cation replacement was substantiated by EDS analyses, as depicted in Fig. 5a and b. The compositional ratios of cobalt and chlorine to carbon (Co/C and Cl/C) derived from the spectra are presented in Fig. 5c and S2 (ESI†). For these EDS measurements, TBDH-Cl was used, since NO_3^- and TFSI$^-$ contain N atoms that cannot be differentiated from the nitrogen in TBDH$^+$ using this technique, whereas the atomic elements in TBDH-Cl differ between the cation and anion. Initially, the as-prepared CNTs showed peaks corresponding to C, O, and Cl. After doping with CoCp*$_2$, a distinct Co peak emerged. Subsequent treatment with TBDH-Cl resulted in a reduction of the Co signal and an increase in the N-related peak, indicating cation replacement. The observed increase in Cl atoms post-TBDH-Cl treatment (Fig. S2) was attributed to unintended adsorption of Cl$^-$ onto the tubes.

To verify the effects of cation replacement, we monitored the changes with time in the Seebeck coefficient and electrical conductivity of CoCp*$_2$-doped and TBDH-X (X$^-$ = Cl$^-$, NO_3^- or TFSI$^-$)-treated CNT films during incubation at 100 °C in air, as shown in Figs. 6 and S3. The temperature (100 °C) was set based on the comparative evaluations using TBD as a dopant, described in more detail in Fig. S4 of ESI†. The Seebeck coefficients of CoCp*$_2$-doped (Fig. 6) and TBDH-TFSI-treated (Fig. S3) samples shifted from negative to positive (indicative of p-type reversion) after incubation periods of 186 and 22 h, respectively. The accelerated dedoping observed in the TBDH-

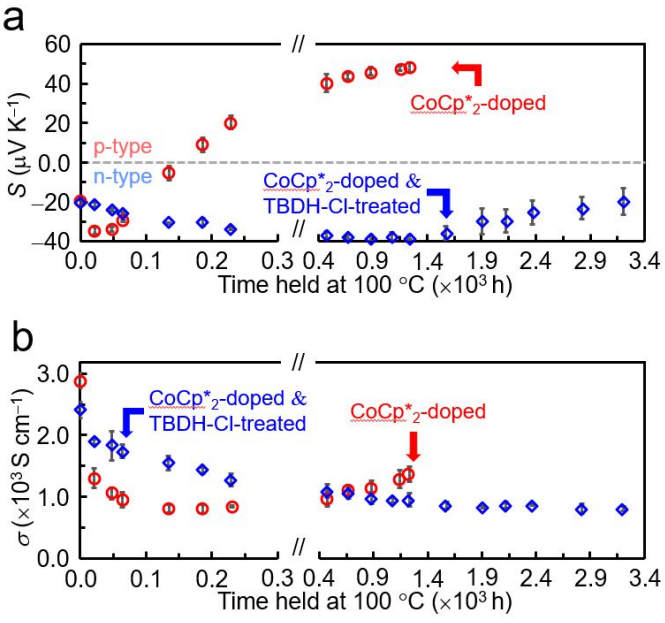

Fig. 6 Variation with time in (a) Seebeck coefficient (S) and (b) electrical conductivity (σ) of CoCp*$_2$-doped and TBDH-Cl-treated CNT films during incubation at 100 °C in air.

TFSI-treated samples is attributed to pre-existing dedoping effects from the salt treatment process. This pattern further confirms that cation replacement was ineffectual in the TBDH-TFSI solution. The electrical conductivity of these samples

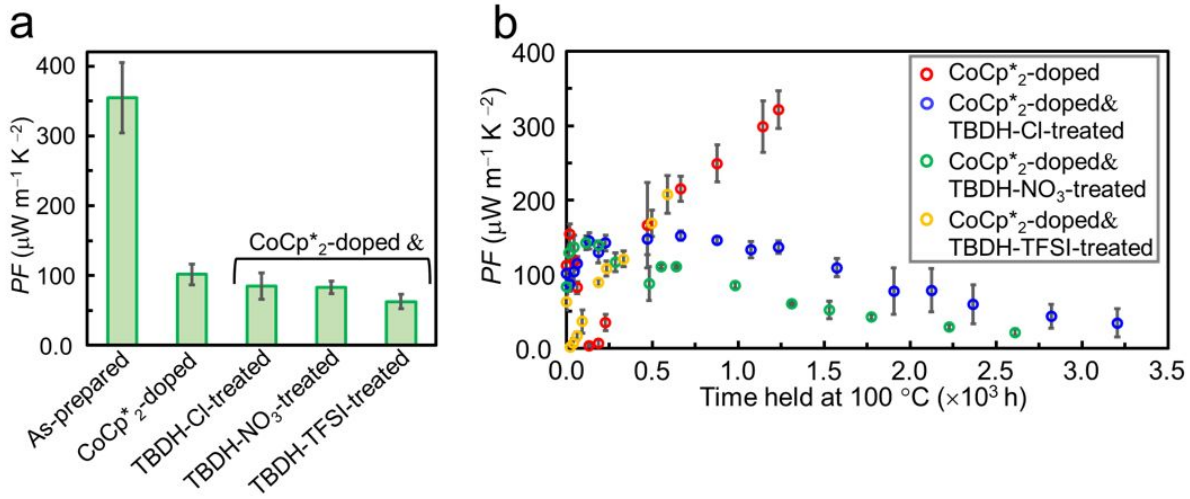

Fig. 7 (a) Thermoelectric power factor (*PF*) before and after $CoCp^*_2$ doping and TBDH-X ($X^- = Cl^-$, NO_3^- or $TFSI^-$) treatments. (b) Temporary changes in power factor (*PF*) of $CoCp^*_2$-doped and TBDH-X ($X^- = Cl^-$, NO_3^- or $TFSI^-$)-treated CNT films during incubation at 100 °C in air. Data statistics: $n = 3$; error bars represent standard deviations. Note that the plots for $CoCp^*_2$-doped CNTs after 186 h (red circle) and $CoCp^*_2$-doped and TBDH-TFSI-treated CNTs after 22 h (orange circle) show the power factors of p-type-reverted samples.

decreased sharply within the initial 0–186 h and 0–22 h periods for the $CoCp^*_2$-doped and TBDH-TFSI-treated samples, respectively, and later stabilized around 1,200 S cm^{-1} after extended incubation. The turning point in conductivity coincides with the moment the Seebeck coefficient indicates a polarity shift from n-type top-type, signaling a transition in the dominant carrier species from electrons to holes.

On the other hand, the CNTs doped with $CoCp^*_2$ and treated with TBDH-Cl (Fig. 6a,b) and TBDH-NO_3 (Fig. S3) demonstrated significant retention of n-type polarity, as evidenced by the preserved negative Seebeck coefficient and the absence of any inflection point in the electrical conductivity over an extended period exceeding 3,200 h (130 d). By comparing the stability of these materials to those of the $CoCp^*_2$-doped and TBDH-TFSI-treated samples, and considering the dedoping trends observed during TBDH-X treatments (Fig. 4), the effectiveness of Cl^- and NO_3^- in facilitating cation replacement is further substantiated.

Moreover, a previous study showed that n-doped CNTs induced by the addition of PEI, a well-known n-type inducer for CNTs, reverted to p-type only after three weeks at 80 °C.[34] This highlights the superior stabilization capability of the TBDH cation in maintaining the n-type character of CNTs.

Here, the other electron doping and stabilization scenarios are taken into considerations: electron donations by Cl^-, neutral TBD residue in the synthesized TBDH-X, or TBD produced by reduction of TBDH by n-doped CNTs and/or $CoCp^*_2$(II) remaining in the CNT films. Nucleophilicity of halogen anion would be enhanced when combined with specific cations by the naked anion effect, as exemplified by crown-ether cations.[28] On the other hand, neutral TBD has the potential to donate electrons to CNTs due to $n \rightarrow \pi^*$ interaction while stabilizing the doped states[26]; unintendedly remained TBD in the salts may contribute to the n-doping and enhanced retention ability of CNTs. TBD molecules produced by the reduction of TBDH by n-type CNTs and/or $CoCp^*_2$(II) during cation replacement process may be also responsible for the electron transfer and stabilization of n-type CNTs by the reported mechanism.[26]

To assess the two former possibilities, we immersed the as-prepared CNT films into acetonitrile solution of TBDH-Cl without the presence of $CoCp^*_2$ and the prior n-doping process. Minimal changes of Seebeck coefficient (+51±1.7 μV K^{-1}) and electrical conductivity (1360±230 S cm^{-1}) compared to the as-prepared samples were confirmed; therefore, TBDH-Cl shows negligible doping ability on CNTs. At the same time, the impact of neutral TBD residue can be also disregarded. Further, treatment by TBDH-NO_3 after $CoCp^*_2$ doping also contributed to the enhanced stability; in this case, the naked anion effect should be excluded. Based on these additional observations and considerations, we have concluded that the chloride anion itself did not have significant impact on doping and stability of CNTs in this material system.

On the other hand, we cannot fully exclude the possibility of electron transfer from n-doped CNTs or residual $CoCp^*_2$ to the $TBDH^+$ cation, potentially leading to the formation of neutral TBD, which may subsequently interact with the CNTs. However, a comparison of the effects of different anions (Cl^-, NO_3^-, and $TFSI^-$) offers important insights. Treatments with TBDH-Cl and TBDH- NO_3 resulted in significantly improved retention of the n-doped state, whereas treatment with TBDH-TFSI failed to provide comparable stability. If neutral TBD formed via reduction of $TBDH^+$ were the main contributor to the enhanced stability, one would expect the TBDH-TFSI treatment to yield a similar effect—yet this was not observed. While we cannot entirely rule out this possibility, the current experimental evidence points more strongly to cation replacement as the dominant factor behind the observed stability enhancement, rather than stabilization via in situ generated neutral TBD.

Finally, we assessed the thermoelectric properties of the doped CNTs, using the Seebeck coefficient and electrical conductivity as metrics to evaluate the predominant carrier types and the retention capabilities of these materials. Development of n-type organic thermoelectric materials with robust performance and stability is one of the research objectives for achieving all-organic thermoelectric

modules.[48,49,50] The relatively large negative Seebeck coefficient and high electrical conductivity of our nanotube samples underscore their potential as n-type thermoelectric materials.

The thermoelectric power factors ($PF = S^2\sigma$) of the CNT films subjected to various treatments, along with their retention capabilities, are depicted in Fig. 7a and b. The power factor for the as-prepared p-type CNT films reached 350 μW m^{-1} K^{-2}, an exceptionally high value for organic materials. The n-doped samples exhibited power factors up to 100 μW m^{-1} K^{-2}, which are considered good to excellent for n-type organic materials (comparison with the literature data is summarized in Table S1 of ESI†). Notably, as illustrated in Fig. 7b, the $CoCp^*_2$-doped and TBDH-TFSI-treated samples experienced significant fluctuations in power factor over the incubation periods of 0–125 h and 0–50 h, respectively. These fluctuations were due to changes in the negative Seebeck coefficients and electrical conductivities (refer to Figs. 6 and S3) and represent a challenge for ensuring stable long-term device performance, especially in energy-harvesting applications.

In contrast, the TBDH-Cl- and TBDH-NO_3-treated samples exhibited much less fluctuation in their power factors, due to the stabilization of both the Seebeck coefficient and electrical conductivity. This stabilization highlights the potential of these materials for use in thermoelectric generators, suggesting that the targeted cation replacements can effectively enhance the durability and performance of n-type thermoelectric materials.

Conclusions

In summary, our study advances ion replacement technology by demonstrating the synthesis of thermally stable n-type CNTs using specific dopants and stabilizer cations through a facile wet process. This approach allows for precise control over electron density and the stabilization of doped states through distinct doping and stabilizing procedures. The superior reduction capability of the cobalt complex was highlighted by the negative Seebeck coefficient, exceptionally high electrical conductivity, and the shift to more negative work functions in the doped CNTs. Good-to-excellent thermoelectric power factors (up to 100 μW m^{-1} K^{-2}) were noted. Additionally, the choice of anion is critical for successful cation replacement, as evidenced by the complex chemistry involved. The n-type CNTs, coordinated with bicyclic-ring guanidinium cations, showed improved thermal stability compared to their as-doped counterparts. However, the cation-replaced n-type CNTs demonstrated some degree of dedoping, as indicated by slight changes in the Seebeck coefficient and electrical conductivity. Partial dedoping was also noted during the cation replacement process. Therefore, future work should focus on exploring stabilizer cations or customizing the molecular structure of TBDH to enhance stability further. In addition, the employed EDS could not quantify the degree of cation replacement due to the small peak intensity of N atom; quantifying the efficiency of ion replacement and associating it with the resulted stability should be also addressed.

Author contributions

S.H. conceived the project. K.K. and S.H. prepared the manuscript under the supervision and guidance of Y.K., A.A., Q.W., and M.F. K.K. performed the synthesis, film preparation, doping, ion replacement, TE characterization, and spectroscopy. All authors contributed to the writing of the manuscript.

Conflicts of interest

The authors declare no competing financial interest.

Data availability

Source data that support the plots within this paper are provided with this paper.

Funding

S.H. acknowledges the support from the JST A-STEP program through Grant No. JPMJTR23R6 and JSPS KAKENHI through Grant No. 23K13671, Japan.

Acknowledgements

The authors thank Prof. A. Mori and Prof. K. Okano for their assistance with the NMR measurements.

References

1 E. Artukovic, M. Kaempgen, D. S. Hecht, S. Roth and G. Grüner, *Nano Lett.*, 2005, **5**, 757–760.
2 T. Chen, L. Qiu, Z. Cai, F. Gong, Z. Yang, Z. Wang and H. Peng, *Nano Lett.*, 2012, **12**, 2568–2572.
3 C. K. Mytafides, L. Tzounis, G. Karalis, P. Formanek and A. S. Paipetis, *ACS Appl. Mater. Interfaces*, 2021, **13**, 11151–11165.
4 M. S. Fuhrer, B. M. Kim, T. Dürkop and T. Brintlinger, *Nano Lett.*, 2002, **2**, 755–759.
5 T. W. Odom, J. Huang, P. Kim and C. M. Lieber, *J. Phys. Chem. B*, 2000, **104**, 2794–2809.
6 K. K. Kim, S. M. Kim and Y. H. Lee, *Acc. Chem. Res.*, 2016, **49**, 390–399.
7 K. Yanagi, S. Kanda, Y. Oshima, Y. Kitamura, H. Kawai, T. Yamamoto, T. Takenobu, Y. Nakai and Y. Maniwa, *Nano Lett.*, 2014, **14**, 6437–6442.
8 M. S. Dresselhaus, G. Dresselhaus and R. Saito, *Carbon*, 1995, **33**, 883–391.
9 R. S. Ruoff and D. C. Lorents, *Carbon*, 1995, **33**, 925-930.
10 H. Hiura, T. W. Ebbesen and K. Tanigaki, *Chem. Phys. Lett.*, 1993, **202**, 509–512.
11 L. Wang, P. Wang, C. Gao, X. Zhao, Q. Dong, D. Chu, W. Bai, Q. Li and Y. He, *J. Mater. Sci.*, 2025, **60**, 4949–4974.
12 S. Yousef and A. Mohamed, *J. Mech. Sci. Technol.*, 2016, **30**, 5135–5141.
13 S. J. Lee, H. K. Baik, J. Yoo, and J. H. Han *Diam. Relat. Mater.*, 2002, **11**, 914–917.
14 T. Tanaka, H. Jin, Y. Miyata and H. Kataura, *Appl. Phys. Express*, 2008, **1**, 114001.
15 T. Yagi, K. Yoshida, S. Sakurai, T. Kawai and Y. Nonoguchi, *J. Am. Chem. Soc.*, 2024, **146**, 20913–20918.
16 R. Krupke, F. Hennrich, H. L. Löhneysen and M. M. Kappes, *Science*, 2003, **301**, 344–347.

17 P. G. Collins, K. Bradley, M. Ishigami and A. Zettl, *Science*, 2000, **287**, 1801–1804.
18 T. M. Barnes, J. L. Blackburn, J. Lagemaat, T. J. Coutts and M. J. Heben, *ACS Nano*, 2008, **2**, 1968–1976.
19 K, Kamarás, Á. Pekker, B. Botka, H. Hu, S. Niyogi, M. E. Itkis and R.C. Haddon, *Phys. Status Solidi B*, 2010, **247**, 2754–2757.
20 S. Ghosh, S R K S. Yamijala, S. K. Pati and C. N. R. Rao, *RSC Adv.*, 2012, **2**, 1181–1188.
21 A. Shawky, J. Nam, K. Kim, J. Han, J. Yoon, S. Seo, C. S. Lee, R. Xiang, Y. Matsuo, H. M. Lee, S. Maruyama and I. Jeon, *Small Methods*, 2021, **5**, 2100080.
22 S. M. Kim, K. K. Kim, Y. W. Jo, M. H. Park, S. J. Chae, D. L. Duong, C. W. Yang, J. Kong and Y. H. Lee, *ACS Nano*, 2011, **5**, 1236–1242.
23 J. Choi, I. A. Samayoa, S. Lim, C. Jo, Y. C. Choi, Y. H. Lee and P. A. Dowben, *Phys. Lett. A*, 2002, **299**, 601–606.
24 J. Lee, J. Yoon, B. Choi, D. Lee, D. M. Kim, D. H. Kim, Y.-K. Choi and S.-J. Choi, *Appl. Phys. Lett.*, 2016, **109**, 263103.
25 Y. Nakashima, R. Yamaguchi, F. Toshimitsu, M. Matsumoto, A. Borah, A. Staykov, M. S. Islam, S. Hayami and T. Fujigaya, *ACS Appl. Nano Mater.*, 2019, **2**, 4703–4710.
26 S. Horike, Q. Wei, K. Akaike, K. Kirihara, M. Mukaida, Y. Koshiba and K. Ishida, *Nat. Commun.*, 2022, **13**, 3517.
27 M. Nishinaka, Q. Wei, Y. Koshiba and S. Horike, *Energy Mater. Adv.*, 2024, **5**, 0123.
28 Y. Nonoguchi, M. Nakano, T. Murayama, H. Hagino, S. Hama, K. Miyazaki, R. Matsubara, M. Nakamura and T. Kawai, *Adv. Funct. Mater.*, 2016, **26**, 3021–3028.
29 Y. Joo, S. Mukherjee and B. W. Boudouris, *ACS Appl. Polym. Mater.*, 2019, **1**, 204–210.
30 Y. Nonoguchi, K. Ohashi, R, Kanazawa, K. Ashiba, K. Hata, C. Adachi, T. Tanase and T. Kawai, *Sci. Rep.*, 2013, **3**, 3344.
31 S. Chang, P. Biswas, Z. Qin and Z. Tian, *Small Methods*, 2024, **8**, 2400585.
32 W. Luo, P. Vishwakarma, C. Hsieh and B. Panigrahi, *Appl. Therm. Eng.*, 2022, **216**, 119142.
33 Y. Liu, J. Yin, P. Wang, Q. Hu, Y. Wang, Y. Xie, Z. Zhao, Z. Dong, J. Zhu, W. Chu, N. Yang, J. Wei, W. Ma and J. Sun, *ACS Appl. Mater. Interfaces*, 2018, **10**, 36304–36311.
34 S. Hata, Y. Yamaguchi, R. Nakata, K. Kametani, Y. Du, Y. Shiraishi and N. Toshima, *Diam. Relat. Mater.*, 2021, **120**, 108656.
35 M. Nishinaka, I. Harada, K. Akaike, Q. Wei, Y. Koshiba, S. Horike and K. Ishida, *Carbon*, 2024, **218**, 118667.
36 Y. Yamashita, J. Tsurumi, M. Ohno, R. Fujimoto, S. Kumagai, T. Kurosawa, T. Okamoto, J. Takeya and S. Watanabe, *Nature*, 2019, **572**, 634–638.
37 Y. Yamashita, S. Kohno, E, Longhi, S. Jhulki, S. Kumagai, S. Barlow, S. R. Marder, J. Takeya and S. Watanabe, *Commun. Mater.*, 2024, **7**, 79.
38 A. Hawkey, A. Dash, X. Rodríguez-Martínez, Z. Zhao, A. Champ, S. Lindenthal, M. Zharnikov, M. Kemerink and J. Zaumseil, *Adv. Mater.*, 2024, **36**, 2404554.
39 X. Zhao, M. Alsufyani, J. Tian, Y. Lin, S. Y. Jeong, H. Y. Woo, Y. Yin and I. McCulloch, *Adv. Mater.*, 2024, **36**, 2412811.
40 M. Xiong, X.-Y. Deng, S.-Y. Tian, K.-K. Liu, Y.-H. Fang, J.-R. Wang, Y. Wang, G. Liu, J. Chen, D. R. Villalva, D. Baran, X. Gu and T. Lei, *Nat. Commun.*, 2024, **15**, 4972.
41 K. Kawasaki, I. Harada, K. Akaike, Q. Wei, Y. Koshiba, S. Horike and K. Ishida, *Commun. Mater.*, 2024, **5**, 21.
42 M. Tedjani, *J. Supercond. Nov. Magn.*, 2021, **34**, 2479–2484.
43 M. Rdest and D. Janas, *Mater.*, 2021, **14**, 65.
44 M. M. Maclnnes, S. Hlynchuk, S. Acharya, N. Lehnert and S. Maldonado, *ACS Appl. Mater. Interfaces*, 2018, **10**, 2004–2015.
45 A. Paul, R. Borrelli, H. Bouyanfif, S. Gottis and F. Sauvage, *ACS Omega*, 2019, **4**, 14780–14789.
46 R. G. Pearson, *J. Am. Chem. Soc.*, 1963, **85**, 3533–3539.
47 T. Ho, *Chem. Rev.*, 1975, **75**, 1–20.
48 H. Tang, Y. Liang, C. Liu, Z. Hu, Y. Deng, H. Guo, Z. Yu, A. Song, H. Zhao, D. Zhao, Y, Zhang, X. Guo, J. Pei, Y. Ma, Y. Cao and F. Huang, *Nature*, 2022, **611**, 271–277.
49 Q. Li, J.-D. Huang, T. Liu, T. P. A. van der Pol, Q. Zhang, S. Y. Jeong, M.-A. Stoeckel, H.-Y. Wu, S. Zhang, X. Liu, H. Y. Woo, M. Fahlman, C.-Y. Yang and S. Fabiano, *J. Am. Chem. Soc.*, 2024, **146**, 15860–15868.
50 C. K. Mytafides, L. Tzounis, G. Karakis, P. Formanek and A. S. Paipetis, *ACS Appl. Mater. Interfaces*, 2021, **13**, 11151–11165.

Data Availability Statement

Source data that support the plots within this paper are provided with this paper.